New Nonlinear Optical Crystal of Rhodamine 590 Acid Phthalate

Nariyangadu, Sesha Bamini; Choedak, Tenzin; Malar, Ezekiel Joy Padma; Chen, Junsheng; Thyrhaug, Erling; Kumar, Pushpendra; Zhou, Jinming; Yechuri, Vidyalakshmi; Pal, Suman Kalyan; Lidin, Sven; Thangadhorai, Kejalakshmy Namassivayane; Karki, Khadga J.; Pullerits, Tönu

Published in:
ACS Omega

DOI:
10.1021/acsomega.0c02303

Publication date:
2020

Document version
Publisher's PDF, also known as Version of record

ACS OMEGA

http://pubs.acs.org/journal/acsodf

Article

New Nonlinear Optical Crystal of Rhodamine 590 Acid Phthalate

Sesha Bamini Nariyangadu,* Tenzin Choedak, Ezekiel Joy Padma Malar,* Junsheng Chen, Erling Thyrhaug, Pushpendra Kumar, Jinming Zhou, Vidyalakshmi Yechuri, Suman Kalyan Pal, Sven Lidin, Kejalakshmy Namassivayane Thangadhorai, Khadga J. Karki, and Tönu Pullerits*

Cite This: *ACS Omega* 2020, 5, 20863−20873

Read Online

ACCESS | Metrics & More | Article Recommendations | Supporting Information

ABSTRACT: The synthesis and crystal structure of rhodamine 590 acid phthalate (RhAP) have been reported. This novel solid-state rhodamine derivative not only has a longer fluorescence lifetime compared to rhodamine solid-state matrixes where emission is quenched but also possesses strong nonlinear optical characteristics. The static and dynamic first- and second-order hyperpolarizabilities were calculated using the time-dependent density functional theory at the B3LYP/6-31+G* level. The computed static values of β and γ of RhAP by the X-ray diffraction (XRD) structure were 31.9×10^{-30} and 199.0×10^{-36} esu, respectively. These values were about 62 times larger than the corresponding values in urea, an already well-known nonlinear optical material. The second-order hyperpolarizability of the compound was determined experimentally by measuring the two-photon absorption cross section using intensity-modulated light fields. The reported compound, excitable at near-infrared, exhibited frequency upconversion with the two-photon absorption coefficient enhanced by two orders of magnitude compared to that of the dye solution. Hosting the dye in the solid, at high concentrations, exploits the nonlinearity of the dye itself as well as results in significant excitonic effects including formation of broad exciton band and superradiance.

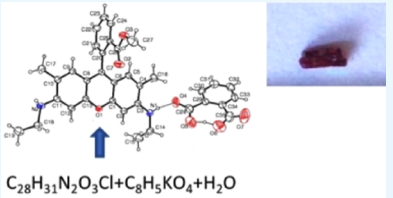

$C_{28}H_{31}N_2O_3Cl+C_8H_5KO_4+H_2O$

Static hyperpolarizability (esu)

Gas phase	RhAP	Urea
$\beta_{\|\|}(0;0,0)$	21.5362D-30	0.314415D-30
$\gamma_{\|\|}(0;0,0,0)$	147.402D-36	3.22137D-36

1. INTRODUCTION

Organic molecular crystals with strong nonlinear optical (NLO) response have received much attention owing to their potential applications in optoelectronics. Applications in optical storage devices and frequency doublers,[1−8] X-ray monochromators, and X-ray analyzers[9−14] have been reported. Large molecular hyperpolarizability is one of the basic requirements for NLO applications. Organic dyes have applications in different fields due to their wide spectral range in the visible region.[15] These dyes can be used in solid, liquid, or gas phases, where their concentration and hence their absorption and gain can be readily controlled. Solid matrixes containing organic laser dyes have been developed with the goal of fabricating practical solid-state dye lasers offering direct access to the visible spectrum at a lower cost. Different solid-state materials like polymers, organic semiconductors, zeolites, sol−gel, and NLO crystals have been used as host media for organic laser dyes. These studies are aimed at the fabrication of dye-doped single-crystal microlasers.[16−29]

Nonlinear organic optical crystals doped with luminescent laser dyes can combine their nonlinear optical property with broadband tunability of the dye.[23−25] Quantum chemical studies have indicated that conjugated heteroaromatic ring systems with extended delocalization of π-electrons exhibit large hyperpolarizability.[30−38] Moreover, the electronic nature and location of heterocyclic rings play a subtle role in the NLO properties of π-conjugated donor−acceptor compounds.[39−42] Although a vast number of nonlinear crystals have been reported in the literature, synthesis of dye-doped crystals has been constrained due to the requirements of transparency, phase-matching, high optical quality, nonlinearity, mechanical stability, photostability, and availability in the bulk form.

Recently, dye-doped metal-free phthalate has been the subject of nonlinear optical studies.[43] The nonlinear optical response in this system arises from the influence of electron clouds of the π-bonds and also from the hyperpolarizability of hydrogen bonds.[44,45] Furthermore, as phthalate belongs to the family of esters, it has been used as a plasticizer for polymers to modify their physical characteristics. Hayden et al. have used esters as a linkage for the preparation of coumarin dye-attached copolymers.[46] Such polymers containing a nonlinear dye moiety can be used in designing a broad set of optical devices like modulators, parametric converters, directional couplers, switches, and lasers. However, it should be noted that hosting the dye in the solid at high concentrations allows us to exploit the nonlinearity of the dye itself. Hence, in this paper, we present the synthesis and properties of a new laser dye crystal, rhodamine 590 acid phthalate. Although different materials

Received: May 17, 2020
Accepted: July 29, 2020
Published: August 10, 2020

https://dx.doi.org/10.1021/acsomega.0c02303
ACS Omega 2020, 5, 20863−20873

have earlier been studied for their nonlinear properties,[47] this new crystal has high optical nonlinearity. To explore the possibility of NLO application of the new rhodamine 590 acid phthalate crystal, we have calculated its (i) first-order and second-order hyperpolarizabilities theoretically by performing quantum chemical computations and (ii) second-order hyperpolarizability experimentally by measuring the two-photon absorption (TPA) cross section using intensity-modulated light fields. Earlier studies have demonstrated that density functional theory (DFT) methods can be successfully used to predict accurate electro-optical properties.[48,49]

2. METHODS

2.1. Single-Crystal X-ray Diffraction (XRD). X-ray diffraction data collection was performed at 293 ± 2 K on an Enraf Nonius CAD4 X-ray diffractometer by standard procedures. The structure solution and refinement were performed by the SHELXL-97 program. The cif file is presented in the SI.

2.2. Optical Measurements. A sample consisting of fine rhodamine−phthalate powder deposited on an optical slide was used for optical experiments. Absorption spectra were recorded on a PerkinElmer lambda 1050 UV/vis/NIR absorption spectrometer. An integrating sphere was used in detection to minimize the distortions from the scattered light. Emission spectra were recorded on a Horiba-Yvon FluoroLog3 spectrometer equipped with a polychromator and a nitrogen-cooled CCD camera. The angle of incidence of the excitation light was set to approximately 60° to minimize the direct scattered light reaching the detector. No dependency on the incidence angle was observed. Time-resolved fluorescence measurements were performed using a time-correlated single-photon counting setup from PicoQuant. A pulsed diode laser with a wavelength of 438 nm was used to excite the sample. The repetition rate of the laser was about 10 MHz, and the pulse duration was about 200 ps. The fluorescence from the sample was collected perpendicular to the excitation beam and directed to a fast avalanche photodiode (SPAD, Micro Photon Devices). The response time of the photodiode was <50 ps. A long-pass filter with a cutoff at 520 nm was used to separate the fluorescence from the scattered laser light.

2.3. Computational Details. *2.3.1. First-Order and Second-Order Hyperpolarizabilities.* We performed DFT calculations on the compound using the B3LYP functional and Pople's split-valence basis set 6-31+G*, which included polarization and diffuse functions on the main group elements as implemented in the Gaussian 09 software.[50] Calculations at the B3LYP/6-31+G* level yield reliable predictions in numerous organic compounds. The molecular and electronic structures of the RhAP were examined by complete structural optimization in the gas phase. In the optimized geometry, the first- and second-order static and dynamic hyperpolarizability tensors were computed using the keywords POLAR = (DCSHG, CUBIC) and CPHF = RDFREQ. The orientationally averaged first-order static hyperpolarizability, β, was calculated from the components of the first hyperpolarizability tensor as[51,52]

$$\beta_{=}\{(\beta_{xxx}+\beta_{xyy}+\beta_{xzz})^2+(\beta_{yyy}+\beta_{yzz}+\beta_{yxx})^2+(\beta_{zzz}+\beta_{zxx}+\beta_{zyy})^2\}^{1/2} \quad (1)$$

The orientationally averaged second-order static hyperpolarizability, γ, was calculated from the components of the second hyperpolarizability tensor as[53−55]

$$\gamma = 1/5\{\gamma_{xxxx}+\gamma_{yyyy}+\gamma_{zzzz}+2[\gamma_{xxyy}+\gamma_{xxzz}+\gamma_{yyzz}]\} \quad (2)$$

The frequency dependence on the first and second (dynamic) hyperpolarizabilities was examined using the tensor components of β $(-2\omega; \omega, \omega)$ and γ $(-2\omega; \omega, \omega, 0)$ at ω = 1064.0 nm. The experimentally relevant first dynamic hyperpolarizability is the parallel component given by

$$\beta_{\parallel}(-2\omega; \omega, \omega) = 1/5 \sum i(\beta zii + \beta izi + \beta iiz) \quad (3)$$

where $i = x, y, z$ and z is oriented toward the direction of the dipole moment of the molecule. The parallel component of γ $(-2\omega; \omega, \omega, 0)$ is defined by the isotropic average

$$\gamma_{\parallel}(-2\omega; \omega, \omega, 0) = (1/15) \sum_{ij} (\gamma_{iijj}+\gamma_{ijij}+\gamma_{ijji}) \quad (4)$$

where $i = x, y, z$ and $\gamma_{\parallel}$ corresponds to the experimentally measurable quantity where the optical field is polarized parallel to the static field. In the static limit $(\omega = 0)$, $\gamma_{\parallel}$ yields eq 2 when the Kleinmann symmetry is applied.

To understand the possibility of the additive relationship, if any, in β and γ, we performed the DFT calculations on the fragments (rhodamine 590 cation and hydrogen phthalate anion) with geometries as in the gas-phase-optimized complex structure. The first and second hyperpolarizabilities in the crystal structure of RhAP were also computed at the B3LYP/6-31+G* level. The results obtained were compared with those for the urea molecule at the same computational level, as crystalline urea finds varied applications as an NLO material and has been extensively studied for its outstanding NLO properties.[56,57]

2.3.2. Transition Dipole Coupling Calculations. For the transition dipole moment, the vertical excitation energy (VEE) calculations[58] were performed from the crystal structure using the TDDFT/B3LYP/TZVP method implemented in the Gaussian 09 program.[50] The coupling strength can be calculated as

$$V = \frac{2\vec{\mu}_1\vec{\mu}_2}{4\pi\varepsilon_0 r^3} \quad (5)$$

Here, $\vec{\mu}_1$ and $\vec{\mu}_2$ are the transition dipole moments in the two neighboring molecules, ε_0 is the vacuum permittivity, and r is the distance between two transition dipole moments.

2.4. Second-Order Hyperpolarizability by Measuring the Two-Photon Absorption Cross Section Using Intensity-Modulated Light Fields. The second-order hyperpolarizability, which is a third-order nonlinear optical process, was deduced experimentally by measuring the two-photon absorption (TPA) coefficient using intensity-modulated light fields. The details of the experimental setup (Figure 1) have been described elsewhere.[59−61] Briefly, a Ti/sapphire oscillator (Synergy from Femtolasers) was used as the optical source (OS). The oscillator produced pulses with a time duration of about 50 fs, which had a bandwidth of about 135 nm and a center wavelength of 790 nm. The repetition rate of the oscillator was about 70 MHz. A pair of chirp mirrors (CMP, Layertec, part number 111298) compensated the group velocity dispersion induced by the different dispersive optical

https://dx.doi.org/10.1021/acsomega.0c02303
ACS Omega 2020, 5, 20863−20873

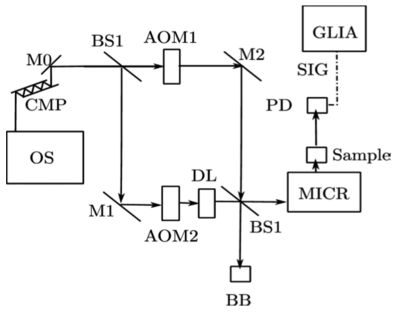

Figure 1. Schematics of the experimental setup used to measure the two-photon absorption cross section of the single crystal of rhodamine 590 acid phthalate. OS, Mode-locked oscillator; CMP, chirp-mirror pair; M, mirror; BS, beam splitter; AOM, acousto-optic modulator; DL, delay line; BB, beam block; PD, photodiode; MICR, microscope; SIG, signal corresponding to the intensity of the beam that has passed the sample; and GLIA, generalized lock-in amplifier.

elements in the setup. The beam was passed into a Mach–Zehnder interferometer setup formed by two 50/50 beam splitters (BSs). The phases of the beams in the two arms of the interferometer were continuously swept at frequencies φ_1 = 54.7 and φ_2 = 54.75 MHz, respectively, using two acousto-optic modulators (AOMs). The difference in the phase modulation frequency was φ_{21} = 50 kHz. A piezo-driven retroreflector (DL) in one of the arms of the interferometer was used to adjust the optimal temporal overlap between the two beams. One of the outputs of the interferometer was sent to a microscope (MICR, Nikon Ti–S), and the other output was blocked by a beam block (BB). A reflective objective was used to focus the beam onto the crystal, and the intensity of the beam that passed through the sample was monitored using a Si photodiode. The photodiode responses at frequencies φ_{21} and 2 φ_{21} were analyzed using a generalized lock-in amplifier (GLIA).[8,62,63]

2.5. Mechanical Characterization by Nanoindentation. Nanoindentation testing was performed using a NanoTest Vantage 4 system (Micro Materials, Ltd., Wrexham, U.K.) with a Berkovich indenter (a radius of 160 nm). At each location, one load cycle was applied up to a maximum load of 20 mN with a loading rate of 2 mN/s and a dwell time of 10 s before unloading at the same speed. The samples were fixed to the bottom of an optically flat disk that was glued onto an aluminum mount using a brittle cyanoacrylate adhesive. An optical microscope was used to identify regions of interest. Depending on the size of the regions, three indents were identified with a minimum distance of 60 μm from neighboring indents. The hardness and modulus of the sample were derived from the measured loading and unloading curves.

3. RESULTS AND DISCUSSION

3.1. Crystal Growth. Growth of the rhodamine 590 acid phthalate crystals was initiated from a concentrated aqueous solution containing dye rhodamine 590 chloride and potassium acid phthalate (KAP) salt. The single crystals of rhodamine 590 acid phthalate (RhAP) were grown in an aqueous solution using the solution growth by slow evaporation at room temperature, as already reported.[24−26] The amount of the dye added to the KAP growth solution was approximately 1% of the amount of KAP salt that was added to the aqueous solution to reach saturation. This was decided by trial and error. Single crystals of rhodamine 590 acid phthalate were synthesized and grown till they reached suitable sizes. They were then harvested. The new single crystals, thus grown, were observed to be intense red in color, as shown in Figure 2. These single crystals were preserved for single-crystal XRD characterizations and optical studies.

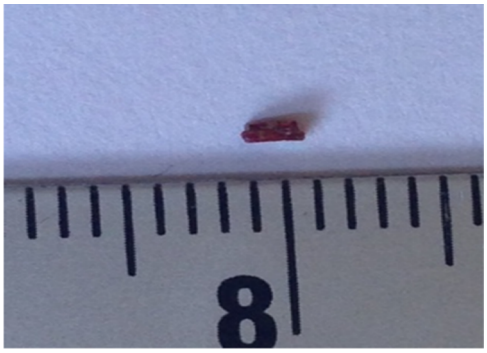

Figure 2. Rhodamine 590 acid phthalate single crystal.

3.2. Single-Crystal XRD. The single-crystal XRD studies (Table 1) revealed that after solvent evaporation from a

Table 1. Crystal Data and Structure Refinement

identification code	Shelxl
empirical formula	C_{35} H_{34} N_2 O_7
formula weight	594.64
temperature	293(2) K
wavelength	0.71073 Å
crystal system, space group	monoclinic, $P21/n$
unit cell dimensions	a = 10.7289(5) Å
	b = 11.1254(5) Å
	c = 25.2451(12) Å
	α = 90°
	β = 91.5020(10)°
	γ = 90°
volume	3012.3(2) Å^3
Z, calculated density	4, 1.311 Mg/m^3
absorption coefficient	0.092 mm^{-1}
F(000)	1256
crystal size	0.35 × 0.35 × 0.30 mm^3
theta range for data collection	2.04–27.49°
limiting indices	$-13 \le h \le 13$, $-14 \le k \le 14$, $-32 \le l \le 32$
reflections collected/ unique	63291/6909 [R(int) = 0.0292]
completeness to θ = 27.49	100.0%
absorption correction	semi-empirical from equivalents
max. and min. transmission	0.9730 and 0.9186
refinement method	full-matrix least-squares on F^2
data/restraints/ parameters	6909/137/464
goodness-of-fit on F^2	1.062
final R indices [$I > \sigma 2(I)$]	R_1 = 0.0526, wR_2 = 0.1402
R indices (all data)	R_1 = 0.0824, wR_2 = 0.1666
largest diff. peak and hole	0.473 and −0.341 e Å^{-3}
symmetry transformations used to generate equivalent atoms	$1 - x + 2$, $-y + 1$, $-z$

https://dx.doi.org/10.1021/acsomega.0c02303
ACS Omega 2020, 5, 20863−20873

saturated solution of KAP, which also contained dye rhodamine 590 chloride, single crystals of the new compound were precipitated out. The systematic name of the compound is xanthylium,9-[2-(methoxycarbonyl)phenyl]-3,6-bis-(ethylamino)-2,7-dimethyl-,hydrogen phthalate (1:1), and its molecular formula is $C_{27}H_{29}N_2O_3$1+, $C_8H_5O_4$1−. The CCDC reference number is CCDC 1010647.

The oak ridge thermal ellipsoid plot (ORTEP) diagram of the single crystal of RhAP is shown in Figure 3A. The ORTEP

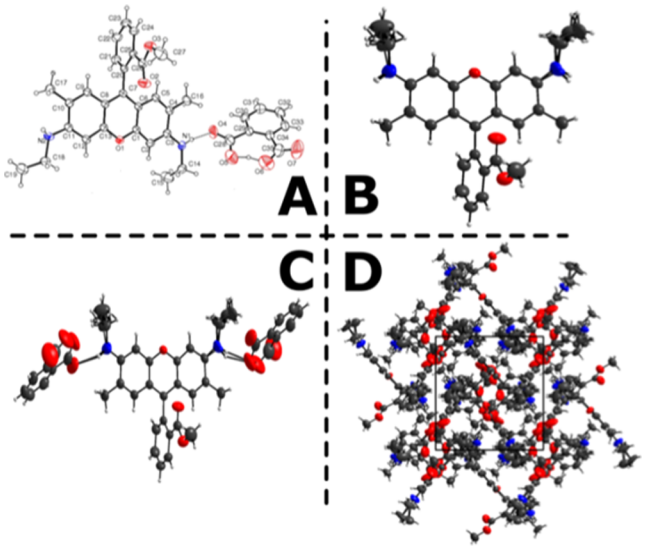

Figure 3. (A) ORTEP diagram of the RhAP crystal. Hydrogen bond between the dye cation and the hydrogen phthalate anion is shown by a dotted line. (B) Single molecule of the title compound oriented with the main planar fragment almost in the plane of vision. The second fragment, the methyl benzoate group, is attached at almost right angles. Note the disorder of the ethyl amide side groups. (C) Weak connections between the molecule of the title compound and the surrounding phthalate groups. The hydrogen bonds are in the interval 2.2−2.6 Å ranging from relatively strong to weak. (D) Molecular packing in the unit cell viewed down the *c* direction of the crystal structure. The perpendicular nature of the association of the two molecular fragments that make up the title compound is obvious.

diagram showed that the potassium ion in the KAP was replaced by the cation of rhodamine 590 chloride. These two moieties were connected via weak hydrogen bonds between the disordered hydrogen H1 and O4, with a H−O distance of about 2.2 Å. The structure of the compound featured two semirigid planar groups that were joined at almost right angles (≈95°). The ethyl amide side groups were partially disordered, which was modeled by split positions for these groups, as illustrated in Figure 3B. The phthalate counter ion was only loosely associated with the main molecule. The shortest intermolecular contact was an O−H distance of around 2.2 Å, corresponding to a weak hydrogen bond (Figure 3C). The molecular packing in the unit cell was best appreciated along the *c*-axis (Figure 3D). All interatomic distances and angles within the molecules were normal.

3.3. First-Order Hyperpolarizability. *3.3.1. DFT Calculations.* The gas-phase geometry of the RhAP generated by complete structural optimization at the B3LYP/6-31+G* level is shown in Figure 4. Clearly, both the experiment and theory revealed that the rhodamine 590 dye cation was bound to the hydrogen phthalate anion through hydrogen-bonding inter-

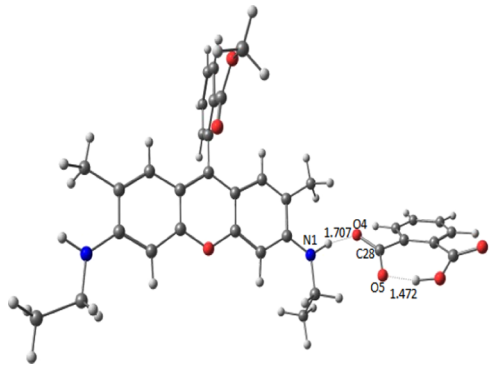

Figure 4. B3LYP/6-31+G*-optimized gas-phase structure of RhAP. The length of the hydrogen bond N1H1···O4 is given in Å. Color code: carbon, gray; nitrogen, blue; oxygen, red; and hydrogen, light gray.

action. Selected structural parameters predicted by the B3LYP/6-31+G* calculation are given along with the corresponding XRD parameters in Table 2.

The structural parameters in Table 2 showed good agreement between the XRD and the predicted gas-phase structure of the complex. However, notable changes were observed in the relative orientation of the two components in the complex. There were differences between the XRD and B3LYP/6-31+G* structural parameters in the region where the hydrogen-bonding interaction occurred. The dihedral angle N1−H1−O4−C28 involving the two components in the complex showed a difference of about 36° between the XRD and B3LYP/6-31+G*-optimized structures (Table 2). This is not unexpected since in the gas phase the complex has more freedom as compared to that in the crystal. It can also be seen that a hydrogen bond length of 1.7 Å predicted for H1···O4 by the DFT calculation was significantly shorter than the corresponding value of 2.19 Å in the RhAP crystal.

The static first-order hyperpolarizability, which is a second-order nonlinear optical property, was computed theoretically. Table 3 lists the ten unique hyperpolarizability components in the third-rank tensor as obtained from the Gaussian 09 software and the total orientationally averaged first-order hyperpolarizability (β). The β predicted for the compound at the B3LYP/6-31+G* level was 34.77 $\times 10^{-30}$ esu. This value was found to be 68 times higher than the first-order hyperpolarizability of urea at the same level as the theory (0.51×10^{-30} esu). Thus, the present analysis showed that the compound can be a good candidate for NLO applications. To check the sensitivity of the first-order hyperpolarizability to the basis set, we also performed the computations using Ahlrichs's triple zeta-valence basis set TZVP[64] at the B3LYP/TZVP level starting from the B3LYP/6-31+G*-optimized geometry. The TZVP basis set resulted in a β value of 34.77×10^{-30} esu, which was identical to the B3LYP/6-31+G* result.

Earlier studies showed that β was sensitive to the geometry of the compound as well as the orientation of donor−acceptor moieties.[48,65] To understand the role of structural variation in the first hyperpolarizability, the B3LYP/6-31+G* calculation was carried out on the crystal structure, which predicted $\beta = 31.94 \times 10^{-30}$ esu (Table 3). The value was reasonably close to the value of 34.77×10^{-30} esu in the gas-phase-optimized structure. Thus, we could infer that the changes in the geometry and orientation in the gas phase and crystal do not alter the first-order hyperpolarizability to any significant extent.

https://dx.doi.org/10.1021/acsomega.0c02303
ACS Omega 2020, 5, 20863−20873

Table 2. Selected Structural Parameters of the Single Crystal of Rhodamine 590 Acid Phthalate Obtained by XRD Study and B3LYP/6-31+G* Structural Optimization in the Gas Phase (Bond Lengths in Å and Bond Angles and Dihedral Angles in Degree)[a] 3

bond length	expt. (XRD)	B3LYP/ 6-31+G*	bond angles	expt. (XRD)	B3LYP/ 6-31+G*
C(1)−C(2)	1.359(2)	1.371	C(2)−C(1)−O(1)	116.83(14)	117.0
C(1)−O(1)	1.3636(19)	1.365	C(2)−C(1)−C(6)	122.92(15)	122.7
C(1)−C(6)	1.415(2)	1.434	O(1)−C(1)−C(6)	120.25(14)	120.3
C(2)−C(3)	1.412(3)	1.428	C(1)−C(2)−C(3)	119.64(16)	120.5
C(3)−N(1)	1.348(3)	1.330	N(1)−C(3)−C(2)	122.5(2)	121.5
C(3)−C(4)	1.437(3)	1.464	N(1)−C(3)−C(4)	117.9(2)	120.0
C(4)−C(5)	1.351(3)	1.366	C(2)−C(3)−C(4)	119.29(16)	118.4
C(5)−C(6)	1.421(2)	1.435	C(5)−C(4)−C(3)	118.76(16)	118.8
C(6)−C(7)	1.389(2)	1.393	C(5)−C(4)−C(16)	120.92(17)	120.8
C(7)−C(8)	1.408(2)	1.427	C(3)−C(4)−C(16)	120.31(17)	120.4
C(8)−C(13)	1.402(2)	1.414	C(4)−C(5)−C(6)	123.47(16)	123.7
C(8)−C(9)	1.413(2)	1.420	C(7)−C(6)−C(1)	119.83(15)	119.4
C(9)−C(10)	1.355(2)	1.378	C(7)−C(6)−C(5)	124.26(15)	124.7
C(10)−C(11)	1.440(2)	1.439	C(1)−C(6)−C(5)	115.90(15)	115.9
C(11)−C(12)	1.392(3)	1.406	Dihedral angles		
C(12)−C(13)	1.375(2)	1.388	C(3)−N(1)−H−O(4)	−146.69	−167.3
C(13)−O(1)	1.364(2)	1.361	N(1)−H−O(4)−C(28)	−82.18	−46.1
C(28)−O(4)	1.215(3)	1.264	H−O(4)−C(28)−C(29)	−158.35	−175.4
C(28)−O(5)	1.269(4)	1.269	C(3)−N(1)−O(4)−C(28)	136.02	149.3
C(28)−C(29)	1.525(3)	1.529	C(6)−C(1)−C(2)−C(3)	−0.9(3)	0.3
C(29)−C(30)	1.382(3)	1.407	C(1)−C(2)−C(3)−N(1)	174.6(3)	178.6
C(29)−C(34)	1.400(3)	1.422	C(2)−C(3)−C(4)−C(5)	0.0(3)	1.1
C(30)−C(31)	1.377(3)	1.392	N(1)−C(3)−C(4)−C(16)	6.4(4)	1.1
C(31)−C(32)	1.369(4)	1.396	C(2)−C(3)−C(4)−C(16)	−179.6(2)	−179.2
C(32)−C(33)	1.362(4)	1.391	C(3)−C(4)−C(5)−C(6)	−0.9(3)	−0.2
C(33)−C(34)	1.379(3)	1.408	C(2)−C(1)−C(6)−C(5)	0.0(3)	0.5
C(34)−C(35)	1.543(4)	1.531	O(4)−C(28)−C(29)−(30)	13.8(3)	−25.8
C(35)−O(7)	1.188(4)	1.223	O(4)−C(28)−C(29)−(34)	−167.4(2)	154.6
C(35)−O(6)	1.258(4)	1.324	O(5)−C(28)−C(29)−(30)	−160.7(3)	151.8
O(5)−H(6A)	1.13(3)	1.492	O(5)−C(28)−C(29)−(34)	18.1(4)	−27.8
O(6)−H(6A)	1.22(3)	1.023	C(28)−C(29)−C(30)−(31)	178.9(2)	−177.9
N(1)−H(1)	0.8600	1.052	C(29)−C(30)−C(31)−(32)	0.8(3)	−1.7
bond angles			C(33)−C(34)−C(35)−(6)	170.0(3)	−160.3
O(4)−C(28)−O(5)	122.5(3)	123.9	C(33)−C(34)−C(35)−(7)	−12.4(4)	17.7
O(4)−C(28)−C(29)	118.5(3)	116.6	hydrogen bond parameters		
O(5)−C(28)−C(29)	118.8(3)	119.5			
C(30)−C(29)−C(34)	118.14 (19)	118.4	H(1)···O(4)	2.19 Å	1.707 Å
C(30)−C(29)−C(28)	114.4(2)	114.3	N(1)···O(4)	3.001(5) Å	2.745 Å
C(31)−C(30)−C(29)	122.3(2)	122.3	N(1)−H(1)−O(4)	157.9°	168.3°
C(32)−C(33)−C(34)	122.7(2)	122.3			
C(32)−C(31)−C(30)	119.1(2)	119.3			
C(33)−C(34)−C(35)	114.6(2)	112.6			
C(33)−C(34)−C(29)	118.4(2)	118.3			

[a]Hydrogen bond parameters are also shown. Atomic labeling as given in Figure 3A was used.

The two components in the title compound, rhodamine 590 cation and the hydrogen phthalate anion, were bound through hydrogen bonding H1···O4 and not through any π-conjugation or covalent bonding. Thus, it can be inferred that the first hyperpolarizability of the new compound under study exhibited an additive relationship. Wu et al.[66] investigated hydrogen bond effects on the polarizability and hyperpolarizability in hydrogen-bonded urea clusters by high-level ab initio calculations. Their study showed that the intermolecular hydrogen-bonding interactions break the additivity for the first hyperpolarizability. We have examined the first hyperpolarizability in the fragments of the title compound using the B3LYP/6-31+G*-optimized gas-phase geometry of the 1:1 complex. The results presented in Table 3 showed that β values for the cation and anion fragments were 32.74×10^{-30} and 2.82×10^{-30} esu, respectively, which add to 35.56×10^{-30} esu. This value is very close to the value of 34.77×10^{-30} esu in the 1:1 complex. Our analysis of the first hyperpolarizability in the title compound conformed to the additive relationship in the hydrogen-bonded system.

Table 4 shows that the parallel component of the first hyperpolarizability $\beta_{\parallel}$ of RhAP at ω = 1064.0 nm has increased 8.8 times in the crystal as compared to the static value. In the gas-phase structure of RhAP, $\beta_{\parallel}$ has increased by 2.3 times when ω = 1064.0 nm.

https://dx.doi.org/10.1021/acsomega.0c02303
ACS Omega 2020, 5, 20863−20873

Table 3. First-Order Static Hyperpolarizability Tensor Components (in Atomic Units, au) and Total First-Order Static Hyperpolarizability β (in au and esu; 1 au = 8.6393 × 10^{-33} esu) as Predicted by DFT Calculations[a]

	RhAP			Rhodamine 590 cation	hydrogen phthalate anion
system	gas-phase-optimized structure		XRD structure	gas phase	gas phase
method	B3LYP/ 6-31+G*	B3LYP/TZVP//B3LYP/6-31+G*	B3LYP/ 6-31+G*	B3LYP/6-31+G*	B3LYP/6-31+G*
β_{XXX}	−2104.46	−2412.69	−2378.17	3197.44	217.84
β_{YXX}	3738.66	3662.37	3333.34	3207.96	17.10
β_{XYY}	902.50	799.45	371.66	−877.85	44.20
β_{YYY}	362.88	255.44	−3.03	2.17	−86.70
β_{ZXX}	−292.41	−252.85	−420.11	−565.69	18.06
β_{XYZ}	−347.85	−348.99	−181.22	6.03	−47.51
β_{ZYY}	−333.14	−293.60	−260.27	−261.76	1.90
β_{XZZ}	66.94	18.54	8.15	−21.61	38.84
β_{YZZ}	−157.52	−120.33	−149.38	−142.05	−6.36
β_{ZZZ}	−21.17	5.52	9.63	46.01	111.78
β (au)	4154.73	4154.10	3815.98	3912.08	337.13
β (10^{-30} esu)	34.77	34.77	31.94	32.74	2.82

[a]esu units = statvolt^{-1} cm^4.

Table 4. Parallel Component of the First Hyperpolarizabilty, $\beta_{\parallel}(-2\omega; \omega, \omega)$ in esu at ω = 0 and 1064.0 nm as Predicted by B3LYP/6-31+G* Calculations in the Gas Phase

	RhAP (gas-phase-optimized structure)	RhAP (XRD structure)	Urea (gas-phase-optimized structure)
$\beta_{\parallel}$ (0; 0, 0)	21.5362D-30	19.7803D-30	0.314415D-30
$\beta_{\parallel}(-2\omega; \omega, \omega)$	49.1341D-30	173.352D-30	0.371558D-30

3.4. Second-Order Hyperpolarizability. *3.4.1. Experimental Determination.* A sensitive and direct loss-modulation scheme was employed to detect the TPA signal. In this method, the intensity of the excitation beam is modulated at a radio frequency φ_{21}. The nonlinearity of two-photon absorption imparts modulation at $2\varphi_{21}$. The power (P_{2F}) of the signal at $2\varphi_{21}$ is measured with respect to the power of the incident beam (P_{1F}). In the measurements, the TPA signals from the title compound at frequency $2\varphi_{21}$ and the modulated amplitude of the incident light at frequency φ_{21} were recorded using the setup as discussed in Section 2.4. With known values of the pulse length (τ), pulse wavelength (λ), sample path length (L), beam radius, photon energy (E), repetition rate of the pulses (f_0), and refractive index (n), the two-photon absorption coefficient of the crystal γ, which is a measure of second-order hyperpolarizability, was calculated using[8]

$$\frac{P_{2F}}{P_{1F}} = \frac{0.66\,\gamma\,n\,E}{\tau\,\lambda\,f_0}\tan^{-1}\left(\frac{L}{2\,n\,Z_0}\right)P_{1F} \quad (6)$$

where Z_0 is the Rayleigh range of the incident beam in the air. The logarithmic plot of the TPA signal gave a slope of 2 (Figure 5a), indicating the quadratic dependence of P_{2F} on the excitation power P_{1F}. This showed that the new compound exhibited efficient two-photon absorption and it can be used in frequency upconversions. Using the slope obtained from Figure 5b and the values of n = 1.67 (refractive index of host matrix KAP), τ = 15 fs, λ = 790 nm, L = 0.01 mm, and Z_0 = 2.3 μm, the TPA coefficient of the new nonlinear optical crystal was deduced to be 6.09 × 10^{-2} cm/GW. The observed two-photon absorption coefficient was found to be two orders of magnitude larger than the corresponding value of 5 × 10^{-4} cm/GW of 30 mM rhodamine 6G in solution.[8]

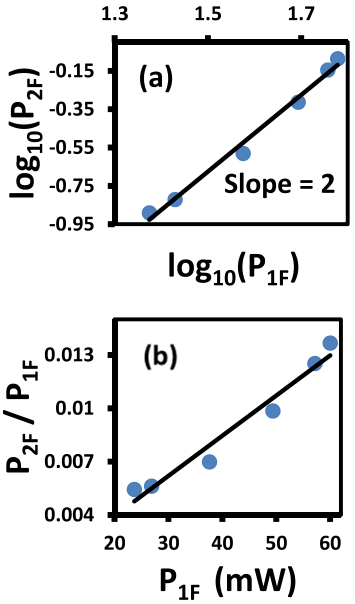

Figure 5. (a) Logarithmic plot of P_{2F} vs P_{1F} and (b) linear dependence of (P_{2F}/P_{1F}) on P_{1F}.

3.4.2. DFT Calculations. The orientationally averaged second-order static hyperpolarizability, γ, and the components of γ for RhAP and its fragments are listed in Table 5. It was remarkable that the second hyperpolarizability in the gas-phase-optimized complex was 147.4 × 10^{-36} esu, which was about 82% more than the sum of the second hyperpolarizabilities in the fragments (81.0 × 10^{-36} esu) possessing the same geometry as in the gas-phase complex structure. This revealed that there was an enhancement of the second hyperpolarizability in the hydrogen-bonded complex unlike the first hyperpolarizability that was found to be additive. Further, as compared to the γ of 60.4 × 10^{-36} esu in rhodamine 590 cation, the γ value was increased by 2.4 times in the complex RhAP. The computed γ of RhAP was based on single-photon excitation, and hence, it could not be compared with the experimentally measured γ of RhAP as the latter was from the two-photon absorption process. Further, the predicted γ in the gas-phase structure of RhAP was about 46 times more than that in urea at the same level of theory. The

https://dx.doi.org/10.1021/acsomega.0c02303
ACS Omega 2020, 5, 20863−20873

Table 5. Orientationally Averaged Second-Order Static Hyperpolarizability γ (in au, esu, and the SI) and Related Components (au) Predicted by Gas-Phase B3LYP/6-31+G* Calculations[a]

	RhAP (gas-phase structure)	RhAP (XRD structure)	Rhodamine 590 cation (gas phase)	hydrogen phthalate anion (gas phase)	urea (gas phase)	urea (gas phase)[b]
γ_{xxxx}	793 467.0	1 348 880.0	162 163.0	61 990.2	9279.2	7380
γ_{yyyy}	171 280.0	166 906.0	158 842.0	20 943.7	3960.9	9760
γ_{zzzz}	87 083.2	83 253.3	54 722.8	36 206.2	5940.6	5920
γ_{xxyy}	135 866.0	114 707.0	65 616.0	11 955.9	3198.9	3240
γ_{xxzz}	33 392.8	37 590.6	18 495.0	20 398.7	1878.2	2960
γ_{yyzz}	36 458.8	35 732.2	27 953.9	10 285.6	1322.4	3630
γ (au)	29 2657.0	395 169.0	11 9971.0	40 884.0	6395.8	8544.0
γ (10^{-36} esu)	147.4	199.0	60.4	20.6	3.2	4.3
γ (10^{-61} SI)	182.5	246.4	74.8	25.5	4.0	

[a]esu unit = statvolt^{-2} cm^5, SI unit = C^4 m^4 J^{-3}. [b]Already published values given in ref 66.

nonlinear properties of urea were extensively studied by Adant et al. and Pluta and Sadlej.[67,68] The static γ of 3.2 × 10^{-36} esu in urea predicted in the present study by the B3LYP method using the 6-31+G* basis set was comparable with the corresponding value of 4.3 × 10^{-36} esu reported by Pluta and Sadlej using the coupled-cluster singles, doubles, and perturbative triples (CCSD(T)) method with the polarized "Pol" basis set.[68−70] It is also interesting to note that the static second hyperpolarizability in the XRD structure of RhAP was 199.0 × 10^{-36} esu, which was about 35% higher than that in the gas-phase structure. The large value of computed second hyperpolarizability in RhAP as compared to that of the NLO candidate urea revealed that RhAP possessed NLO property.

The parallel component of the dynamic second hyperpolarizability $\gamma_{\parallel}$ $(-2\omega; \omega, \omega, 0)$ at ω = 1064.0 nm in RhAP obtained by the B3LYP/6-31+G* calculations in the gas phase was compared with the static value $\gamma_{\parallel}$ (0; 0, 0, 0) in Table 6. A large increase in the magnitude of $\gamma_{\parallel}$ with frequency was observed. This was in agreement with earlier reports.[54]

Table 6. Parallel Component of the Second Hyperpolarizability $\gamma_{\parallel}$ $(-2\omega; \omega, \omega, 0)$ in esu at ω = 0 and 1064.0 nm as Predicted by B3LYP/6-31+G* Calculations in the Gas Phase

	RhAP (gas-phase structure)	RhAP (XRD structure)	urea (gas-phase structure)
$\gamma_{\parallel}$(0; 0, 0, 0)	147.402D-36	199.035D-36	3.22137D-36
$\gamma_{\parallel}$ $(-2\omega; \omega, \omega, 0)$	1322.75D-36	−1104.10D-36	3.96297D-36

3.5. TDDFT of Exciton Coupling. The transition dipole moment of the molecule in the crystal was obtained by TDDFT calculations based on the crystal structure, as shown in Figure 6. The calculated transition dipole moments of the two neighboring molecules ($S_0 \rightarrow S_1$) are shown in Figure 6. The transition dipole moment coupling strength was calculated as explained in Section 2.3.2 using eq 5. The coupling strength was found to be 515.7 cm^{-1} in the RhAP crystal.

3.6. Photophysical Properties. The absorption and emission spectra of a microcrystalline sample of RhAP are shown in Figure 7. The absorption lineshape of the crystal was significantly broader compared to the growth solution spectrum of RhAP, with the typically pronounced vibronic structure only weakly observable. The absorption maximum was at approximately 540 nm, i.e., about the same as the growth solution spectrum. The distortions to the lineshape can

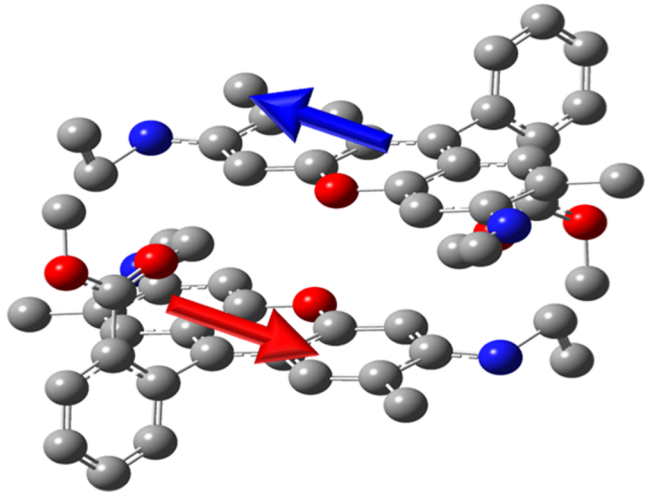

Figure 6. Calculated $S_0 \rightarrow S_1$ transition dipole moment (blue arrow) from (0, 0, 0) to (−3.2267, −0.0399, −0.0908) and the neighboring molecule's $S_0 \rightarrow S_1$ transition dipole moment (red arrow) from (−6.15520000, −3.2202, 3.667) to (−2.9285, −3.1803, 3.7578000).

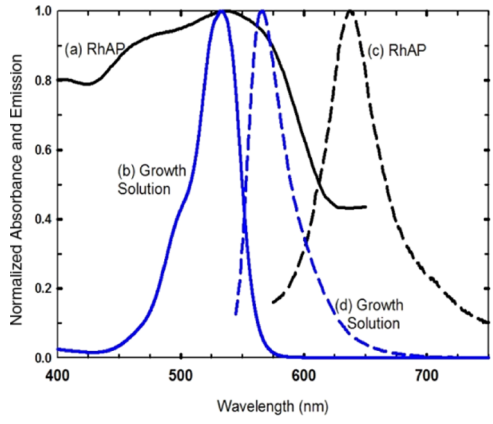

Figure 7. (a, b) Normalized absorbance (solid lines) and (c, d) normalized emission (dashed lines) spectra of RhAP crystal and growth solution.

be at least partly because the sample, which although microcrystalline, was inhomogeneous and consisted of very strongly absorbing crystallites. This type of sample can lead to "flattened" spectral profiles in bulk measurements.[71] However, most of the broadening was a result of the considerable exciton coupling. The nearest-neighbor configuration in Figure 6

https://dx.doi.org/10.1021/acsomega.0c02303
ACS Omega 2020, 5, 20863−20873

resembles an H-aggregate and would lead to absorption at higher energies compared to the monomeric absorption. However, the crystal structure (see Figure 3D) was more complex, having also obvious head-to-tail and perpendicular mutual orientations of the pigments, leading to a generally broadened excitonic absorption spectrum. We have not carried out any precise exciton calculation of the whole crystal, but the nearest-neighbor exciton coupling obtained in the previous section can lead to a rather broad exciton band. The fluorescence spectrum of the RhAP crystal had a maximum at approximately 630 nm. This was red-shifted by about 2000 cm^{-1} relative to the growth solution spectrum, as seen in Figure 7. Emission mainly comes from the significantly red-shifted lowest exciton band. However, the nearest-neighbor exciton coupling of about 500 cm^{-1} cannot explain the whole red shift. Consequently, part of the shift is likely to come from structural reorganization leading to polaron formation.[72]

The fluorescence lifetimes of the RhAP single crystal (Figure 8a) and its growth solution (Figure 8b), measured using the

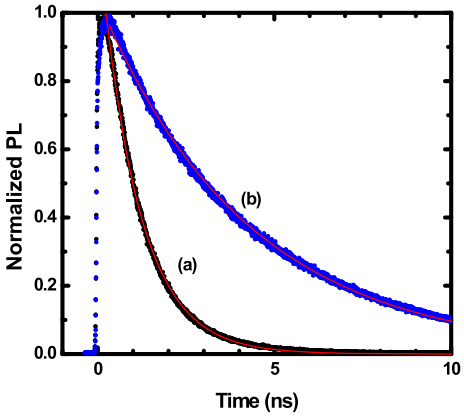

Figure 8. Fluorescence decay profile of (a) RhAP crystal (black dots) and (b) growth solution (blue dots).

TCSPC technique, were 1.1 and 4.2 ns, respectively. The fourfold reduction of the fluorescence lifetime can be attributed to the exciton delocalization leading to enhanced collective radiative dipole moment and the corresponding superradiance.[73−75] It should be noted that the previously reported quenched fluorescence has a lifetime of about 45 ps for the rhodamine B multilayer system, attributed to fast nonradiative decay induced by coupling to the lattice modes available in a multilayer system.[76,77]

3.7. Mechanical Characterization. The mechanical characterization experiment was carried out as explained in Section 2.5. Typical loading−unloading curves were obtained when indenting the specimen (RhAP) up to a maximum load of 20 mN and are presented in Figure 9a. The pop-out of the unloading curve around 2250 nm depth suggested that during unloading the pressure released caused a transformation from the original structure into an amorphous one, within the indentation—affected zone presented in Figure 9b.[65] The experimentally determined modulus and hardness of the new NLO RhAP crystal were found to be 15 and 3.5 GPa, respectively.

4. CONCLUSIONS

A new nonlinear optical crystal was synthesized in an aqueous solution using a simple solution growth technique at room

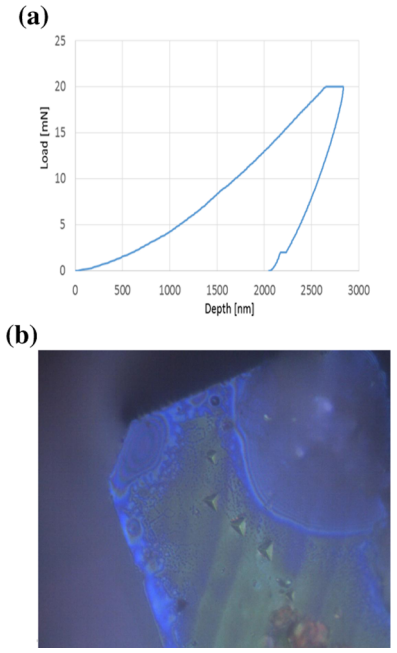

Figure 9. (a) Load−depth curve of the RhAP crystal and (b) microscopic image of RhAP at the nanoindentation-affected zone.

temperature by including an organic laser dye at high concentrations into the KAP crystal. Single-crystal XRD studies revealed the formation of a new compound. Photophysical characterizations on the new NLO crystal demonstrated significant excitonic effects including the formation of a broad exciton band and superradiance due to the enhanced collective radiative dipole moment. Both the experiment and theory revealed that the rhodamine 590 dye cation was bound with the hydrogen phthalate anion through hydrogen-bonding interaction and not through any π-conjugation or covalent bonding. The first- and second-static hyperpolarizabilities (β and γ) predicted for the title compound at the B3LYP/6-31+G* level using the XRD structure were 31.94×10^{-30} and 199×10^{-36} esu, respectively. The above β and γ values in the title compound are about 62 times higher than the corresponding values of urea (0.51×10^{-30} and 3.2×10^{-36} esu) predicted at the same level of the theory. The dynamic $\beta_{||}$ and $\gamma_{||}$ of RhAP, computed at the XRD structure as well as the B3LYP/6-31+G*-optimized gas-phase structure, are of high magnitudes at ω = 1064 nm as compared to the corresponding static values at ω = 0 nm. The large values of the computed first and second hyperpolarizabilities in RhAP as compared to those of the NLO candidate urea revealed that RhAP possessed NLO properties. The two-photon absorption coefficient of the title compound was experimentally found to be 6.09×10^{-2} cm/GW using intensity-modulated light fields, which was two orders of magnitude higher than that of rhodamine 6G in the solution. The title compound exhibited quadratic dependence of power of the TPA signal on that of the incident light. Hence, it was inferred that the new crystal can be used in frequency upconversions as it was a good candidate for two-photon absorption processes. It was concluded from the present analysis that the new solid-state compound, called rhodamine 590 acid phthalate crystal, exhibited impressive NLO properties and hence is a good candidate for applications.

https://dx.doi.org/10.1021/acsomega.0c02303
ACS Omega 2020, 5, 20863−20873

■ ASSOCIATED CONTENT

Supporting Information

The Supporting Information is available free of charge at https://pubs.acs.org/doi/10.1021/acsomega.0c02303.

RhAP crystal structure solution and refinement CIF format; B3LYP/6-31+G*-optimized (gas-phase) Cartesian coordinates, in angstrom, of the rhodamine 590 acid phthalate complex; cartesian coordinates, in angstrom, of the XRD structure, supplied by SAIF; rhodamine 590 cation fragment extracted from the B3LYP/6-31+G(D)-optimized geometry of the complex; and hydrogen phthalate anion fragment extracted from the B3LYP/6-31+G(D)-optimized geometry of the complex (PDF)

RhAP crystal (CIF)

■ AUTHOR INFORMATION

Corresponding Authors

Sesha Bamini Nariyangadu − *Chemical Physics and NanoLund, Lund University, 22100 Lund, Sweden; National Centre for Ultrafast Processes, University of Madras, Chennai 600113, India;* orcid.org/0000-0002-1264-5194; Email: seshabamini@hotmail.com

Ezekiel Joy Padma Malar − *National Centre for Ultrafast Processes, University of Madras, Chennai 600113, India;* orcid.org/0000-0001-5643-4498; Email: ejpmalar@yahoo.com

Tönu Pullerits − *Chemical Physics and NanoLund, Lund University, 22100 Lund, Sweden;* orcid.org/0000-0003-1428-5564; Email: tonu.pullerits@chemphys.lu.se

Authors

Tenzin Choedak − *National Centre for Ultrafast Processes, University of Madras, Chennai 600113, India*

Junsheng Chen − *Chemical Physics and NanoLund, Lund University, 22100 Lund, Sweden; Nano-Science Center & Department of Chemistry, University of Copenhagen, 1165 København, Denmark;* orcid.org/0000-0002-2934-8030

Erling Thyrhaug − *Chemical Physics and NanoLund, Lund University, 22100 Lund, Sweden*

Pushpendra Kumar − *Chemical Physics and NanoLund, Lund University, 22100 Lund, Sweden; School of Basic Sciences, Indian Institute of Technology, Mandi 175005, India*

Jinming Zhou − *Department of Production and Materials Engineering, Lund University, 22100 Lund, Sweden*

Vidyalakshmi Yechuri − *Department of Physics, Anna University, Chennai 600025, India*

Suman Kalyan Pal − *School of Basic Sciences, Indian Institute of Technology, Mandi 175005, India;* orcid.org/0000-0003-2498-6217

Sven Lidin − *Division of Polymer and Materials Chemistry, Lund University, 22100 Lund, Sweden;* orcid.org/0000-0001-9057-8233

Kejalakshmy Namassivayane Thangadhorai − *Photonics Modelling Group, City University, London EC1V 0HB, U.K.*

Khadga J. Karki − *Chemical Physics and NanoLund, Lund University, 22100 Lund, Sweden;* orcid.org/0000-0002-0002-4163

Complete contact information is available at: https://pubs.acs.org/10.1021/acsomega.0c02303

Notes

The authors declare no competing financial interest.

■ ACKNOWLEDGMENTS

S.B.N. acknowledges DST-PURSE, India, SC-XRD LAB, SAIF IITM, India, for data collection and structure solution. S.B.N. acknowledges the Carl Tryggers Foundation in Stockholm (Project CTS 15:399) for supporting this work. E.J.P.M. thanks Dr. Douglas Fox, Gaussian Inc., Wallingford, USA, for valuable discussions regarding second-order hyperpolarizability calculations. J.C. acknowledges the Lundbeck Foundation (grant R303-2018-3237). T.P. acknowledges the Swedish Research Council, Swedish Energy Agency, KAW Foundation, and NanoLund.

■ ABBREVIATIONS USED

RhAP, rhodamine 590 acid phthalate; β, first-order static hyperpolarizability; γ, second-order static hyperpolarizability

■ REFERENCES

(1) Nalwa, H. S.; Miyata, S. *Nonlinear Optics of Organic Molecules and Polymers*; CRC Press: Boca Raton, FL, 1997.

(2) Shi, Y.; Zhang, C.; Zhang, H.; Bechtel, J. H.; Dalton, L. R.; Robinson, B. H.; Steier, W. H. Low (sub-1 Volt) halfwave polymeric electro-optic modulators achieved by controlling chromophore shape. *Science* **2000**, *288*, 119−122.

(3) Zyss, J. *Molecular Nonlinear Optics: Materials, Physics and Devices*; Academic Press: Boston, 1994.

(4) Prasad, P. N.; Williams, D. J. *Introduction to Nonlinear Optical Effects in Molecules and Polymers*; Wiley: Chichester, 1991.

(5) Kanis, D. R.; Ratner, M. A.; Marks, T. J. Design and construction of molecular assemblies with large second-order optical nonlinearities. Quantum chemical aspects. *J. Chem. Rev.* **1994**, *94*, 195−242.

(6) Mortazavi, M. A.; Higgins, B. G.; Dienes, A.; Knoesen, A.; Kowel, S. T. Second-harmonic generation and absorption studies of polymer-dye films oriented by corona-onset poling at elevated temperatures. *J. Opt. Soc. Am. B* **1989**, *6*, 733−741.

(7) Jones, J. L.; Paschen, K. W.; Nicholson, J. B. Performance of Curved Crystals in the Range 3 to 12A. *Appl. Opt.* **1963**, *2*, 955−961.

(8) Tian, P.; Warren, W. S. Ultrafast measurement of two-photon absorption by loss modulation. *Opt. Lett.* **2002**, *27*, 1634−1636.

(9) Charbonnier, M.; Romand, M.; Grubis, B. New organic crystals as x-ray monochromators: Triphenylbenzene and thallium tartrate. *X-Ray Spectrom.* **1988**, *17*, 149−154.

(10) Kejalakshmy, N.; Srinivasan, K. Electro-optic properties of potassium hydrogen phthalate crystal and its application as modulators. *J. Phys. D: Appl. Phys.* **2003**, *36*, 1778−1782.

(11) Belyaev, L. M.; Belikova, G. S.; Gil'varg, A. B.; Sil'vestrova, I. M. The growth of potassium hydrogen phthalate crystals and their optical, piezoelectric and elastic properties. *Sov. Phys. Crystallogr.* **1970**, *14*, 544−549.

(12) Varma, K. B. R.; Raychaudhuri, A. K. Pyroelectric and dielectric properties of potassium hydrogen phthalate single crystals. *J. Phys. D: Appl. Phys.* **1989**, *22*, 809−811.

(13) Kejalakshmy, N.; Srinivasan, K. Growth, optical and electro-optical characterisations of potassium hydrogen phthalate crystals doped with Fe3+ and Cr3+ ions. *Opt. Mater.* **2004**, *27*, 389−394.

(14) Okaya, Y. The crystal structure of potassium acid phthalate, $KC_6H4COOH.COO$. *Acta Crystallogr.* **1965**, *19*, 879−882.

(15) Schafer, F. P. *Dye Lasers*; Springer-Verlag: Berlin, 1975.

(16) Soffer, B. H.; McFarland, B. B. Continuously tunable, narrow-band organic dye lasers. *Appl. Phys. Lett.* **1967**, *10*, 266−267.

(17) Sesha Bamini, N.; Ramalingam, A.; Gowri, V. S.; Rekha, R. K. Spectral and laser studies on energy transfer binary dye-doped polymer laser rods. *J. Mod. Opt.* **2008**, *55*, 2911−2928.

(18) Sesha Bamini, N.; Ramalingam, A.; Gowri, V. S. Comparative Photophysical and energy transfer studies of C480:C535 binary dye mixture in solid and liquid environments. *J. Lumin.* **2010**, *130*, 1011−1020.

(19) Sesha Bamini, N.; Ramalingam, A.; Gowri, V. S. Effect of different donors and a polymer environment on photophysical and energy transfer studies using C540 as the acceptor. *Pramana* **2012**, *79*, 1503−1524.
(20) Tang, C. W.; Vanslyke, S. A. Organic electroluminescent diodes. *Appl. Phys. Lett.* **1987**, *51*, 913−915.
(21) Vietze, U.; Krauß, O.; Laeri, F.; Ihlein, G.; Schüth, F.; Limburg, B.; Abraham, M. Zeolite-dye microlasers. *Phys. Rev. Lett.* **1998**, *81*, 4628−4631.
(22) Qiu, F.; Xu, H.; Cao, Y.; Jiang, Y.; Zhou, Y.; Liu, J.; Zhang, X. Nonlinear optical materials: Synthesis, characterizations, thermal stability and electro-optical properties. *Mater. Charact.* **2007**, *58*, 275−283.
(23) Benedict, J. B.; Wallace, P. M.; Reid, P. J.; Jang, S.-H.; Kahr, B. Up-conversion luminescence in dye-doped crystals of potassium hydrogen phthalate. *Adv. Mater.* **2003**, *15*, 1068−1070.
(24) Enculescu, M. Morphological and optical properties of doped potassium hydrogen phthalate crystals. *Phys. B* **2010**, *405*, 3722−3727.
(25) Enculescu, M.; Matei, E.; Perda, N.; Enculescu, I. Growth and optical characteristics of coumarin 6 doped potassium hydrogen phthalate (KAP) crystals. *Optoelectronics and Adv. Mater. Rapid Comm.* **2009**, *3*, 1210−1212.
(26) Sesha Bamini, N.; Vidyalakshmi, Y.; Choedak, T.; Kejalakshmy, N.; Muthukrishnan, P.; Ancy, C. J. Synthesis, linear optical, non-linear optical, thermal and mechanical characterizations of dye-doped semi-organic NLO crystals. *Mater. Res. Exp.* **2015**, *2*, No. 065010.
(27) Braun, I.; Ihlein, G.; Laeri, F.; Nöckel, J. U.; Schulz-Ekloff, G.; Schüth, F.; Vietze, U.; Weiss, Ö.; Wöhrle, D. Hexagonal microlasers based on organic dyes in nanoporous crystals. *Appl. Phys. B: Lasers Opt.* **2000**, *70*, 335−344.
(28) Ihlein, G.; Schüth, F.; Krauß, O.; Vietze, U.; Laeri, F. Alignment of a laser dye in the channels of the AlPO 4-5 molecular sieve. *Adv. Mater.* **1998**, *10*, 1117−1119.
(29) Tomazio, N. B.; Boni, L. D.; Mendonca, C. R. Low threshold Rhodamine-doped whispering gallery mode microlasers fabricated by direct laser writing. *Sci. Rep.* **2017**, *7*, No. 8559.
(30) Skwara, B.; Go′ra, R. W.; Zales′ny, R.; Lipkowski, P.; Bartkowiak, W.; Reis, H.; Papadopoulos, M. G.; Luis, J. M.; Kirtman, B. Electronic structure, bonding, spectra and linear and non-linear electric properties of Ti @ C28. *J. Phys. Chem. A* **2011**, *115*, 10370−10381.
(31) Loboda, O.; Zaleśny, R.; Avramopoulos, A.; Luis, J.-M.; Kirtman, B.; Tagmatarchis, N.; Reis, H.; Papadopoulos, M. G. Linear and nonlinear optical properties of [60] fullerene derivatives. *J. Phys. Chem. A* **2009**, *113*, 1159−1170.
(32) Karabacak, M.; Karaca, C.; Atac, A.; Eskici, M.; Karanfil, A.; Kose, E. Synthesis, analysis of spectroscopic and nonlinear optical properties of the novel compound: (S)-N-benzyl-1-phenyl-5-(thiophen-3-yl)-4-pentyn-2-amine. *Spectrochim. Acta, Part A* **2012**, *97*, 556−567.
(33) Rao, V. P.; Jen, A. K.-Y.; Wong, K. Y.; Drost, K. J. Novel push-pull thiophenes for 2nd order nonlinear optical applications. *Tetrahedron Lett.* **1993**, *34*, 1747−1750.
(34) Jen, A. K.-Y.; Cai, Y. M.; Bedworth, P. V.; Marder, S. R. Synthesis and characterization of highly efficient and thermally stable diphenylamino-substituted thiophene stilbene chromophores for nonlinear optical applications. *Adv. Mater.* **1997**, *9*, 132−135.
(35) Cho, B. R.; Son, K. N.; Lee, S. J.; Kang, T. I.; Han, M. S.; Jeon, S. J.; Song, N. W.; Kim, D. First-order hyperpolarizabilities of 2-[2-(p-diethylaminophenyl) vinyl]-furan derivatives. *Tetrahedron Lett.* **1998**, *39*, 3167−3170.
(36) Song, S.; Lee, S. J.; Cho, B. R.; Shin, D.-H.; Park, K.-H.; Lee, C. J.; Kim, N. Side-chain nonlinear optical polymers containing a styrylfuran-based chromophore with large electro-optic properties. *Chem. Mater.* **1999**, *11*, 1406−1408.
(37) Shu, C.-F.; Wang, Y.-K. Synthesis of nonlinear optical chromophores containing electron-excessive and deficient heterocyclic bridges. The auxiliary donor-acceptor effects. *J. Mater. Chem.* **1998**, *8*, 833−835.
(38) Brasselet, S.; Cherioux, F.; Audebert, P.; Zyss, J. New octupolar star-shaped structures for quadratic nonlinear optics. *Chem. Mater.* **1999**, *11*, 1915−1920.
(39) Varanasi, P. R.; Jen, A. K. Y.; Chandrasekhar, J.; Namboothiri, I. N. N.; Rathna, A. The important role of heteroaromatics in the design of efficient second-order nonlinear optical molecules: theoretical investigation on push-pull heteroaromatic stilbenes. *J. Am. Chem. Soc.* **1996**, *118*, 12443−12448.
(40) Albert, I. D. L.; Marks, T. J.; Ratner, M. A. Large molecular hyperpolarizabilities. Quantitative analysis of aromaticity and auxiliary donor-acceptor effects. *J. Am. Chem. Soc.* **1997**, *119*, 6575−6582.
(41) Breitung, E. M.; Shu, C.-F.; McMahon, R. J. Thiazole and thiophene analogues of donor-acceptor stilbenes: molecular hyperpolarizabilities and structure-property relationships. *J. Am. Chem. Soc.* **2000**, *122*, 1154−1160.
(42) Sunitha, M. S.; Vishnumurthy, K. A.; Adhikari, A. V. Synthesis and two-photon absorption property of new pi-conjugated donor-acceptor polymers carrying different heteroaromatics. *J. Chem. Sci.* **2013**, *125*, 29−40.
(43) Kaminskii, A. A.; Bagayev, S. N.; Dolbinina, V. V.; Voloshin, A. E.; Rhee, H.; Eichler, H. J.; Hanuza, J. Potassium and ammonium hydrogen phthalates KHC6H4(COO)2 and (NH4)HC6H4(COO)2 − New organic crystals for Raman laser converters with large frequency shift. *Laser Phys. Lett.* **2009**, *6*, 544−551.
(44) Dirk, C. W.; Twieg, R. J.; Wagniere, G. The contribution of pi electrons to second harmonic generation in organic molecules. *J. Am. Chem. Soc.* **1986**, *108*, 5387−5395.
(45) Chemla, D. S. *Nonlinear Optical Properties of Organic Molecules and Crystals*; Elsevier, 2012.
(46) Hayden, L. M.; Sauter, G. F.; Ore, O. F.; Pasillas, P. L.; Hoover, J. M.; Lindsay, G. A.; Henry, R. A. Second-order nonlinear optical measurements in guest-host and side-chain polymers. *J. Appl. Phys.* **1990**, *68*, 456−465.
(47) Nisha, B.; Vidyalakshmi, Y.; Geetha, D.; Ruhena Parveen, J.; Vinitha, G. Green synthesis, characterization of silver nanoparticles and their study on antibacterial activity and optical limiting behaviour. *Appl. Phys. B* **2019**, *125*, No. 123.
(48) Jug, K.; Chiodo, S.; Calaminici, P.; Avramopoulos, A.; Papadopoulos, M. G. Electronic and vibrational polarizabilities and hyperpolarizabilities of azoles: A comparative study of the structure-polarization relationship. *J. Phys. Chem. A* **2003**, *107*, 4172−4183.
(49) Calaminici, P.; Jug, K.; Köster, A. M.; Ingamells, V. E.; Papadopoulos, M. G. Polarizabilities of azabenzenes. *J. Chem. Phys.* **2000**, *112*, 6301−6308.
(50) Frisch, M. J.; Trucks, G. W.; Schlegel, H. B.; Scuseria, G. E.; Robb, M. A.; Cheeseman, J. R.; Scalmani, G.; Barone, V.; Mennucci, B.; Petersson, G. A.; Nakatsuji, H.; Caricato, M.; Li, X.; Hratchian, H. P.; Izmaylov, A. F.; Bloino, J.; Zheng, G.; Sonnenberg, J. L.; Hada, M.; Ehara, M.; Toyota, K.; Fukuda, R.; Hasegawa, J.; Ishida, M.; Nakajima, T.; Honda, Y.; Kitao, O.; Nakai, H.; Vreven, T.; Montgomery, J. A., Jr.; Peralta, J. E.; Ogliaro, F.; Bearpark, M.; Heyd, J. J.; Brothers, E.; Kudin, K. N.; Staroverov, V. N.; Keith, T.; Kobayashi, R.; Normand, J.; Raghavachari, K.; Rendell, A.; Burant, J. C.; Iyengar, S. S.; Tomasi, J.; Cossi, M.; Rega, N.; Millam, J. M.; Klene, M.; Knox, J. E.; Cross, J. B.; Bakken, V.; Adamo, C.; Jaramillo, J.; Gomperts, R.; Stratmann, R. E.; Yazyev, O.; Austin, A. J.; Cammi, R.; Pomelli, C.; Ochterski, J. W.; Martin, R. L.; Morokuma, K.; Zakrzewski, V. G.; Voth, G. A.; Salvador, P.; Dannenberg, J. J.; Dapprich, S.; Daniels, A. D.; Farkas, O.; Foresman, J. B.; Ortiz, J. V.; Cioslowski, J.; Fox, D. J. *Gaussian 09*, revision D.01; Gaussian, Inc.: Wallingford, CT, 2013.
(51) Thanthiriwatte, K. S.; de Silva, K. M. N. Non-linear optical properties of novel fluorenyl derivatives- ab initio quantum chemical calculations. *J. Mol. Struct.: THEOCHEM* **2002**, *617*, 169−175.
(52) Srinivasan, P.; Vidyalakshmi, Y.; Gopalakrishnan, R. Studies on the synthesis, growth, crystal structure and nonlinear optical properties of a novel nonlinear optical crystal: L-Argininium-4-nitro

https://dx.doi.org/10.1021/acsomega.0c02303
ACS Omega 2020, 5, 20863−20873

phenolate monohydrate (LARP). *Cryst. Growth Des.* **2008**, *8*, 2329−2334.
(53) Kurtz, H. A.; Stewart, J. J. P.; Dieter, K. M. Calculation of the nonlinear optical properties of molecules. *J. Comput. Chem.* **1990**, *11*, 82−87.
(54) Kongsted, J.; Osted, A.; Mikkelsen, K. V.; Christiansen, O. Second harmonic generation second hyperpolarizability of water calculated using the combined coupled cluster dielectric continuum or different molecular mechanics methods. *J. Chem. Phys.* **2004**, *120*, 3787−3798.
(55) Boggard, M. P.; Orr, B. J. *MTP International Review of Science, Physical Chemistry*; Butterworths: London, 1975.
(56) Halbout, J. M.; Tang, C. L. *Nonlinear Optical Properties of Organic Molecules and Crystals*; Academic Press: New York, 1987.
(57) Champagne, B.; Bishop, D. M. Calculating non-linear optical properties for the solid-state. *Adv. Chem. Phys.* **2003**, *126*, 41−92.
(58) Chen, J.-S.; Zhao, F.-J.; Yang, Y.; Chu, T. S. Hydrogen bond effect on the photophysical properties of 2-ureido-4[1H]-pyrimidinone quadruple hydrogen bonded systems. *RSC Adv.* **2015**, *5*, 36279−36287.
(59) Karki, K. J.; Kringle, L.; Marcus, A. H.; Pullerits, T. Phase-synchronous detection of coherent and incoherent nonlinear signals. *J. Opt.* **2016**, *18*, No. 015504.
(60) Osipov, V. A.; Shang, X.; Hansen, T.; Pullerits, T.; Karki, K. J. Nature of relaxation processes revealed by the action signals of intensity-modulated light fields. *Phys. Rev. A* **2016**, *94*, No. 053845.
(61) Karki, K.; Torbjörnsson, M.; Widom, J. R.; Marcus, A. H.; Pullerits, T. Digital cavities and their potential applications. *J. Instrum.* **2013**, *8*, No. T05005.
(62) Fu, S.; Sakurai, A.; Liu, L.; Edman, F.; Pullerits, T.; Öwall, V.; Karki, K. J. Generalized lock-in amplifier for precision measurement of high frequency signals. *Rev. Sci. Instrum.* **2013**, *84*, No. 115101.
(63) Jin, A.; Fu, S.; Sakurai, A.; Liu, L.; Edman, F.; Pullerits, T.; Öwall, V.; Karki, K. J. Note: High precision measurements using high frequency gigahertz signals. *Rev. Sci. Instrum.* **2014**, *85*, No. 126102.
(64) Weigend, F.; Ahlrichs, R. Balanced basis sets of split valence and quadruple zeta valence quality for H to Rn: Design and assessment of accuracy. *Phys. Chem. Chem. Phys.* **2005**, *7*, 3297−3305.
(65) Tapily, K.; Gu, D.; Baumgart, H.; Namkoong, G.; Stegall, D.; Elmustafa, A. A. Mechanical and structural characterization of atomic layer deposition-based ZnO films. *Semicond. Sci. Technol.* **2011**, *26*, No. 115005.
(66) Wu, K.; Snijders, J. G.; Lin, C. Reinvestigation of hydrogen bond effects on the polarizability and hyperpolarizability of urea molecular clusters. *J. Phys. Chem. B* **2002**, *106*, 8954−8958.
(67) Adant, C.; Dupuis, M.; Bre'das, J. L. Ab initio study of the nonlinear optical properties of urea:Electron correlation and dispersion effects. *Int. J. Quantum Chem.* **1995**, *S29*, 497−507.
(68) Pluta, T.; Sadlej, A. J. Electric properties of urea and thiourea. *J. Chem. Phys.* **2001**, *114*, No. 136.
(69) Sadlej, A. J. Medium-size polarized basis sets for high-level correlated calculations of molecular electric properties. *Collect. Czech. Chem. Commun.* **1988**, *53*, 1995−2016.
(70) Sadlej, A. J. Medium-size polarized basis sets for high-level correlated calculations of molecular electric properties II. Second-row atoms Si-Cl. *Theor. Chim. Acta* **1991**, *79*, 123−140.
(71) Tian, Y.; Scheblykin, I. G. Artifacts in absorption measurements of organometal halide perovskite materials. What are the real spectra? *J. Phys. Chem. Lett.* **2015**, *6*, 3466−3470.
(72) Polívka, T.; Pullerits, T.; Herek, J. L.; Sundstrom, V. Exciton relaxation and polaron formation in LH2 at low temperature. *J. Phys. Chem. B* **2000**, *104*, 1088−1096.
(73) Schröter, M.; Pullerits, T.; Kühn, O. Using fluorescence detected two-dimensional spectroscopy to investigate initial exciton delocalization between coupled chromophores. *J. Chem. Phys.* **2018**, *149*, No. 114107.
(74) Dahlbom, M.; Pullerits, T.; Mukamel, S.; Sundström, V. Exciton delocalization in the B850 light-harvesting complex: Comparison of different measures. *J. Phys. Chem. B* **2001**, *105*, 5515−5524.
(75) Monshouwer, R.; Abrahamsson, M.; van Mourik, F.; van Grondelle, R. Superradiance and exciton delocalization in bacterial photosynthetic light-harvesting systems. *J. Phys. Chem. B* **1997**, *101*, 7241−7248.
(76) Kemnitz, K.; Tamai, N.; Yamazaki, I.; Nakashima, N.; Yoshihara, K. Fluorescence decays and spectral properties of rhodamine B in submono-, mono- and multilayer systems. *J. Phys. Chem. A.* **1986**, *90*, 5094−5101.
(77) Alnayli, R. S.; Shanon, Z. S.; Hadi, A. S. Study the Linear and Nonlinear Optical Properties for Laser Dye Rhodamine B. *J. Phys.: Conf. Ser.* **2019**, *1234*, 012022−012032.

https://dx.doi.org/10.1021/acsomega.0c02303
ACS Omega 2020, 5, 20863−20873